AMERICAN SOCIETY FOR MICROBIOLOGY | Journal of Virology®

VIRUS-CELL INTERACTIONS

Tunneling Nanotubes as a Novel Route of Cell-to-Cell Spread of Herpesviruses

Mirosława Panasiuk,[a] Michał Rychłowski,[a] Natalia Derewońko,[a] Krystyna Bieńkowska-Szewczyk[a]

[a]Laboratory of Virus Molecular Biology, Intercollegiate Faculty of Biotechnology, University of Gdańsk, Gdańsk, Poland

ABSTRACT Various types of intercellular connections that are essential for communication between cells are often utilized by pathogens. Recently, a new type of cellular connection, consisting of long, thin, actin-rich membrane extensions named tunneling nanotubes (TNTs), has been shown to play an important role in cell-to-cell spread of HIV and influenza virus. In the present report, we show that TNTs are frequently formed by cells infected by an alphaherpesvirus, bovine herpesvirus 1 (BoHV-1). Viral proteins, such as envelope glycoprotein E (gE), capsid protein VP26, and tegument protein Us3, as well as cellular organelles (mitochondria) were detected by immunofluorescence and live-cell imaging of nanotubes formed by bovine primary fibroblasts and oropharynx cells (KOP cells). Time-lapse confocal studies of live cells infected with fluorescently labeled viruses showed that viral particles were transmitted via TNTs. This transfer also occurred in the presence of neutralizing antibodies, which prevented free entry of BoHV-1. We conclude that TNT formation contributes to successful cell-to-cell spread of BoHV-1 and demonstrate for the first time the participation of membrane nanotubes in intercellular transfer of a herpesvirus in live cells.

IMPORTANCE Efficient transmission of viral particles between cells is an important factor in successful infection by herpesviruses. Herpesviruses can spread by the free-entry mode or direct cell-to-cell transfer via cell junctions and long extensions of neuronal cells. In this report, we show for the first time that an alphaherpesvirus can also spread between various types of cells using tunneling nanotubes, intercellular connections that are utilized by HIV and other viruses. Live-cell monitoring revealed that viral transmission occurs between the cells of the same type as well as between epithelial cells and fibroblasts. This newly discovered route of herpesviruses spread may contribute to efficient transmission despite the presence of host immune responses, especially after reactivation from latency that developed after primary infection. Long-range communication provided by TNTs may facilitate the spread of herpesviruses between many tissues and organs of an infected organism.

KEYWORDS Tunneling nanotubes, TNT, herpes, BoHV-1, bovine herpesvirus 1, cell-to-cell transmission

Cells can communicate in a variety of ways, ranging from the secretion of soluble factors into the environment to direct contacts and cellular projections linking individual cells. The diversity of such intercellular connections makes their classification difficult, and the nomenclature of various protrusions involved in cell communication or cell migration may be sometimes confusing, although these protrusions differ in morphological, structural, and functional characteristics (reviewed in references 1 to 3). Advanced imaging techniques have recently made it possible to visualize a new type of intercellular connections: fragile, elongated structures that can transiently connect distant cells, sometimes for a very short time. Such membrane protrusions, named

Received 19 January 2018 **Accepted** 12 February 2018

Accepted manuscript posted online 28 February 2018

Citation Panasiuk M, Rychłowski M, Derewońko N, Bieńkowska-Szewczyk K. 2018. Tunneling nanotubes as a novel route of cell-to-cell spread of herpesviruses. J Virol 92:e00090-18. https://doi.org/10.1128/JVI.00090-18.

Editor Rozanne M. Sandri-Goldin, University of California, Irvine

Address correspondence to Krystyna Bieńkowska-Szewczyk, krystyna.bienkowska-szewczyk@biotech.ug.edu.pl.

tunneling nanotubes (TNTs), were described for the first time for cultured rat pheochromocytoma PC12 cells (4). They were initially characterized as thin (50 to 200 nm in diameter), long, membranous channels composed of actin filaments and containing no tubulin. Later, the formation of similar membrane connections was observed in other cultured cells, such as human embryonic kidney (HEK-293) cells (5), normal rat kidney (NRK) cells (4, 6), HeLa cells (7), neurons and astrocytes (8, 9), and many others (reviewed in references 3 and 10). Numerous observations have demonstrated that nanotubes can connect immune cells, macrophages, monocytes, natural killer (NK) cells, or Epstein-Barr virus (EBV)-transformed human B cells (11). Such "tubes" connect the cytoplasm of cells and allow the exchange of signals, materials, and organelles (lysosomes and mitochondria) between nonadjacent cells. Recent studies have shown that the morphologies and compositions of TNTs formed by various cells may differ. For example, two distinct types of tunneling nanotubes connecting human macrophages have been described: thin nanotubes containing only actin and thicker (diameter over 0.7 μm) bridges containing both actin and microtubules (12). There is no clear hallmark defining TNTs, and their length can vary from 10 to more than 100 μm. Observations of TNTs both *in vitro* and *in vivo* are technically difficult because these structures are sensitive to light, mechanical stress, and chemical fixation. Any one of those can cause visible vibrations of the tubular connection and rupture, and therefore, the search for TNTs in living tissues is a challenging task. Most studies on TNTs have been performed *in vitro* using cultured cells, whereas observations of TNTs *in vivo* have rarely been published: some examples include sea urchin embryos (13), myeloid cells in mouse cornea (14, 15), and the region between the neural crest in chicken embryo (16). However, large amounts of evidence indicate that TNT-mediated communication and transport are essential for normal cell functioning under physiological conditions (17). The molecular mechanism of membrane nanotube formation is not fully understood, but stressful conditions, such as inflammation or any cell injury, have been shown to stimulate cells to produce TNTs (18).

A growing number of reports have demonstrated the important role of TNTs in the pathogenesis of neurodegenerative diseases and cancer (19), and the field of TNT research is rapidly widening. A significant factor that may contribute to TNT formation is the interaction of the cell with the pathogen. Tunneling nanotubes of various dimensions have been shown to be involved in the transmission of bacteria (12), prions (20, 21), and viruses. The first report about viral transmission in TNTs was described for the spread of human immunodeficiency virus (HIV) from infected T cells to an uninfected one using nanotubular connections (22, 23). This new route of HIV transmission was later confirmed by observations of HIV dissemination *in vivo* within lymph nodes of humanized mice (24). "Hijacking" of TNTs and other cellular communication pathways by HIV enhances viral transmission to large populations of cells and is considered an important factor in HIV neuropathogenesis and in the establishment of viral reservoirs (25). Moreover, the HIV accessory protein Nef has been shown to stimulate the formation of tunneling nanotubes and virological synapses (26).

The involvement of TNTs in the spread of viral infection was recently reported for other RNA viruses: influenza virus (IAV) (27) and porcine reproductive and respiratory syndrome virus (PRRSV) (28). For both viruses, viral proteins and replication components were detected in actin-rich connections formed by a variety of cells: Vero cells, HEK-293T cells, BHK-21 cells, and porcine macrophages for PRRSV and MDCK cells, A549 cells, and primary human bronchial epithelial cells for IAV.

In the present study, we investigated whether a DNA virus, an alphaherpesvirus, could also utilize nanotubular connections during infection. A hallmark of all herpesvirus infections is the ability to establish latent infection. During latency, the virus is hidden from the host immune response developed during the primary infection, but after reactivation, herpesviruses survival depends on an efficient strategy to circumvent host immune defenses (29–31). Direct transmission via closed cell-cell contacts is an important strategy of herpesvirus immune evasion. Alphaherpesviruses can spread across the junctions between the membranes of cells or by fusion of adjacent cells, and

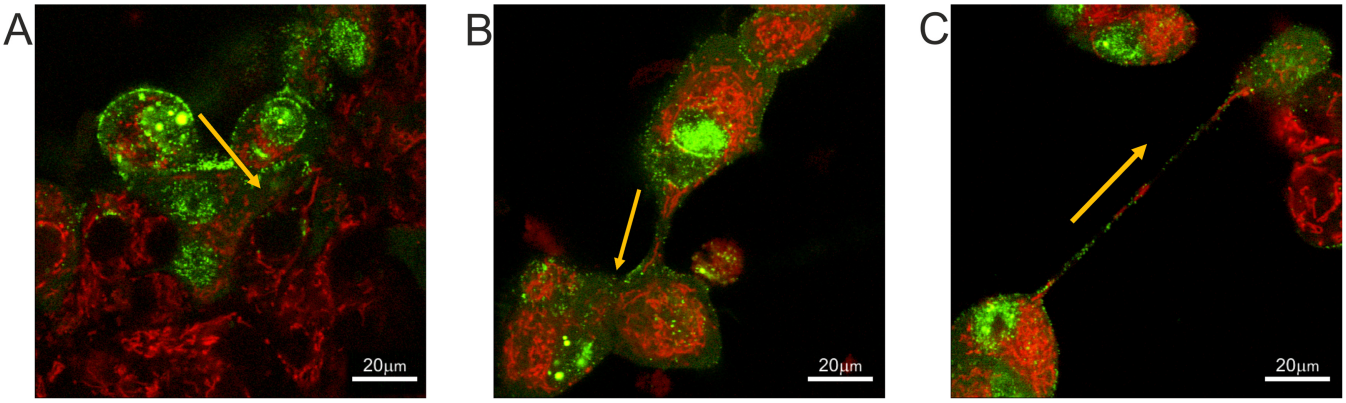

FIG 1 Transfer of cellular and viral components between cells through different types of cell connections. (A) Direct cell junctions; (B) thick cellular bridge; (C) tunneling nanotube. MDBK cells were infected with BoHV-1-VP26-GFP (green) and stained with MitoTracker red to visualize mitochondria (red). Yellow arrows indicate the main direction of viral transfer. See also Movies S1 and S2 in the supplemental material. Images and time-lapse movies were obtained using a Nikon PCM2000 confocal microscope.

they travel "long distances" along neurons (32, 33). Neuronal spread requires the transfer of virions across neural synapses and the transport of viral particles within axons to the sensory ganglia. The major target cells of alphaherpesviruses are epithelial cells (where primary infection usually starts) and neurons, where they persist during latency. However, apart from these two target cells, alphaherpesviruses are able to infect many types of cells *in vitro* and *in vivo*. This flexibility is mediated by the complex interaction of multiple viral glycoproteins and cellular receptors (34), providing the virus with diverse routes of entry and spread.

Our model alphaherpesvirus, bovine herpesvirus 1 (BoHV-1), is a widespread bovine pathogen, a member of the *Varicellovirus* genus of *Alphaherpesvirinae*. BoHV-1 shares many features with human herpesviruses, such as herpes simplex virus 1 (HSV-1) and varicella-zoster virus (VZV) (35). Due to its strong immunomodulatory properties, BoHV-1 is an interesting model for studies of viral immune evasion and cell-to-cell spread (36, 37). BoHV-1 has a restricted host range compared with those of other herpesviruses; the natural host of BoHV-1 is cattle, and it is propagated in cells of bovine origin, although it has recently been shown to also infect human tumor cells (38). In our studies of BoHV-1 entry and transmission, we often observed that infected cells produced a network of cellular projections with various diameters and lengths. Some of these extensions had a morphology characteristic of TNTs, and we wanted to determine whether viral particles or proteins could be found in these connections.

In this study, we used bovine cells with a limited life span, primary fibroblasts and epithelial cells, to investigate BoHV-1 infection. Cells with a limited life span reflect the more natural and authentic course of infection, as opposed to typical cell lines such as MDBK. First, we characterized the connections formed by uninfected cells and confirmed the presence of TNT-like structures in both cell types. Searching for viral proteins in tubular conduits formed by BoHV-1-infected cells resulted in the detection of structural components of the viral envelope, capsid, and tegument. The live-cell imaging results for cells infected with fluorescent BoHV-1 with tags attached to capsid or envelope (or to both viral compartments) indicated that TNTs could be involved in cell-to-cell spread of herpesvirus.

RESULTS

Various types of cell connections are observed between BHV-1-infected cells. In our studies of BoHV-1 entry and transmission, we used various cell types: commonly used laboratory cell lines (e.g., MDBK), a panel of epithelial cell strains with a limited life span (EBTR and KOP), and primary fibroblasts isolated from calf skin. Virus transfer between directly adjacent cells could be easily visualized in all types of cells (Fig. 1A). We also frequently observed (using fluorescently labeled virus, BoHV-1-VP26-GFP) the

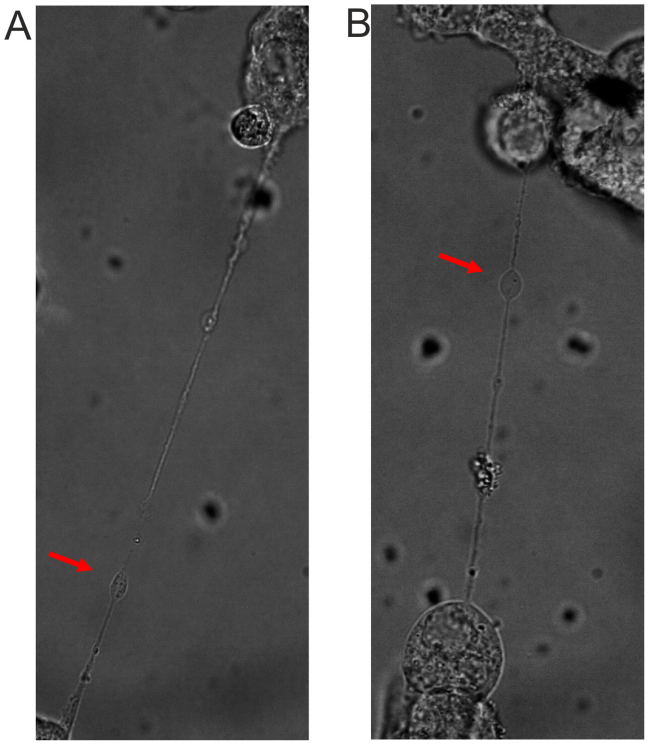

FIG 2 Bright-field images of tunneling nanotubes formed between BoHV-1-infected MDBK (A) and KOP (B) cells with visible vesicles (gondolas). Red arrows indicate vesicle structures. Images were obtained using a Nikon PCM2000 confocal microscope.

transmission of viral proteins through intercellular connections of various diameters and lengths, which were rapidly formed between infected cells. In cell cultures with a high density of seeded cells, the majority of the connections looked like thick short bridges (Fig. 1B; see also Movie S1 in the supplemental material). However, we also often observed the formation of thinner, elongated structures, which were more prevalent in less densely seeded cell cultures (Fig. 1C; see also Movie S2). The morphology of these longer tubular connections matched the description of membrane tunneling nanotubes (TNTs). These actin-containing projections were fragile, thin, and long (often more than 100 μm). They floated freely in the medium without attaching to the substratum. Fluorescence analysis in living cells revealed the transfer of labeled mitochondria and green fluorescent protein (GFP)-tagged viral proteins from one cell to another via these long connections. The transfer of cytoplasmic molecules suggests membrane continuity between two connected cells, which is one of the main features of tunneling nanotubes. Bright-field imaging showed that granules and vesicle-like structures (also described as gondolas) formed inside nanotubes from one cell to another (Fig. 2).

Thin membrane connections formed between cultured bovine cells of various origin have features characteristic of TNTs. To confirm that the observed connections could be classified as TNTs, we investigated the projections formed by the two types of cells chosen for our further studies: bovine oropharynx epithelial cells (KOP) and primary bovine fibroblasts. Both types of cells divide a limited number of times, retain (to some extent) the characteristics of their source tissue, and are very useful for examinations of the time course of events during viral infection. First, we characterized the intercellular connections in uninfected cells (Fig. 3). TNTs do not have any specific markers, but they differ from other cell projections by their morphological properties. They contain F-actin (sometimes tubulin as well) and are long and fragile. To characterize the connections formed by the bovine cells used in our experiments, we decided to analyze their structural composition. However, the highly dynamic and transient

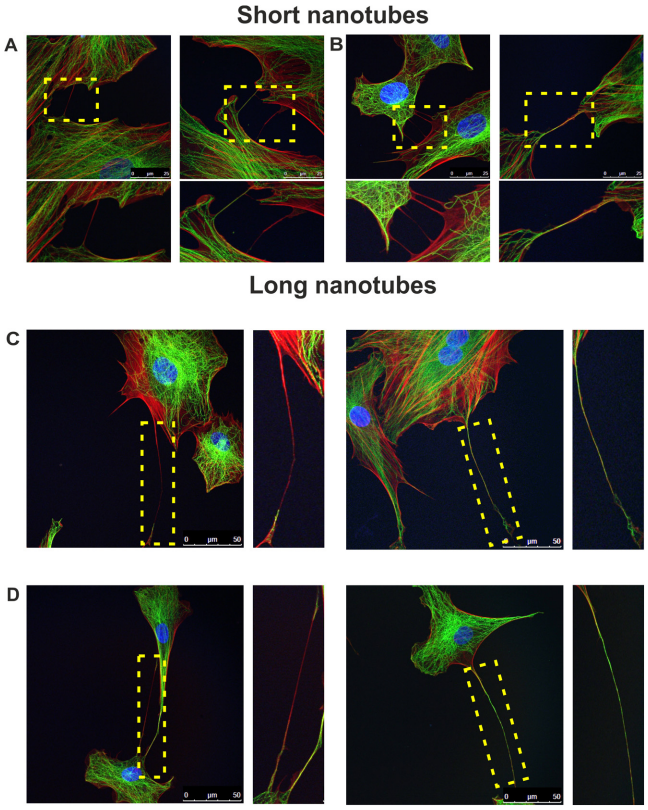

FIG 3 Tunneling nanotubes connect cells of bovine origin. Uninfected KOP cells (A and C) and bovine fibroblasts (B and D) were fixed and stained to observe F-actin (red), α-tubulin (green), and nuclei (blue). Based on their lengths, nanotubes were classified as short (A and B) or long (C and D). Zoomed images of nanotubes (boxed regions) are shown under each picture in the top row (A and B) and at the right of the images in the bottom row (C and D). Images were obtained using a Leica TCS Sp8 X confocal microscope. Scale bars: 25 μm (top row) and 50 μm (bottom row).

nature of those connections and their mechanical and chemical sensitivity made it difficult to perform immunofluorescence experiments. Initial experiments using a 4% paraformaldehyde (PFA) and glutaraldehyde-formaldehyde mixture for cell fixation did not provide satisfying results due to the breakage of most of the fragile connections. We improved the fixation method by adding 16% PFA directly to the medium above the cells to a final concentration of 4% PFA. This technique, along with very delicate handling of the samples, allowed fixation of the cells without disruption of the TNTs and immunofluorescence analysis in a reproducible manner. We observed nanotubes of various lengths which we classified as short ($\leq$20 μm) or long ($>$20 μm). Using anti-α-tubulin antibody and phalloidin-tetramethyl rhodamine isocyanate (TRITC) (a high-affinity filamentous F-actin probe), we analyzed different types of intercellular connections. Some of them (mostly short nanotubes) consisted only of actin fibers. Most of the very long connections (some over 110 μm) contained both actin filaments and microtubules (Fig. 3). These projections were not attached to the substratum but seemed to be floating in the medium. The observations of the morphology, formation, and composition of long intercellular membrane bridges between the investigated cells convinced us that they were membrane nanotubes linking distant cells.

The presence of BoHV-1 in TNTs detected by immunofluorescence. To determine whether nanotubes were involved in the process of BoHV-1 infection, we performed a series of immunofluorescence experiments. KOP cells and bovine fibroblasts were infected with wild-type BoHV-1. At 12 h postinfection (h.p.i.), the cells were fixed and analyzed for the presence of virus protein with anti-BoHV-1 serum. Additionally, the cells were also stained for F-actin, which was previously shown to be present in all types of nanotubes.

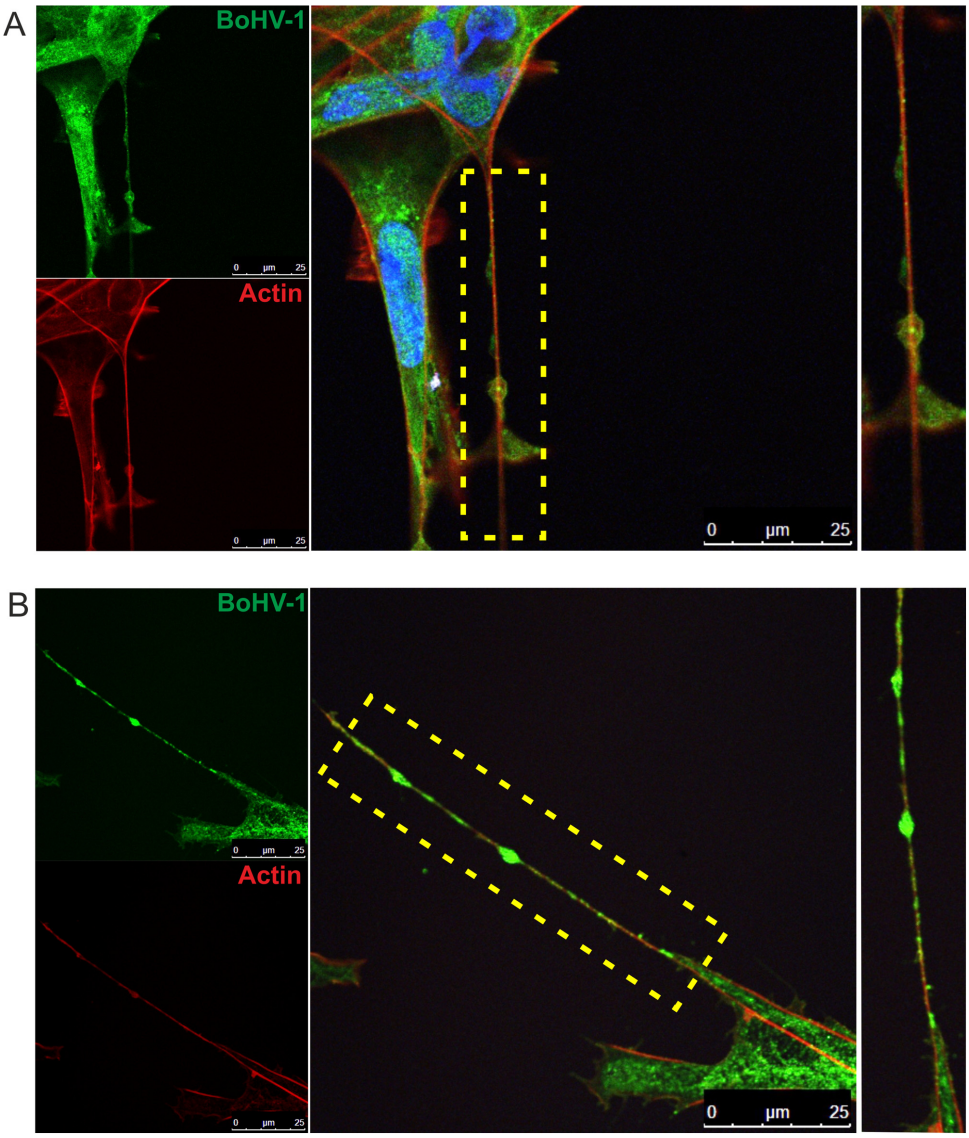

FIG 4 Detection of BoHV-1 in tunneling nanotubes. KOP cells (A) and bovine fibroblasts (B) were infected with BoHV-1-WT (MOI = 1). At 12 h.p.i., the cells were fixed and stained. BoHV-1 proteins were detected using anti-BoHV-1 serum (green staining). Additionally, the cells were stained for F-actin (red staining) and nuclei (blue staining). Zoomed images of nanotubes (boxed regions) are shown at the right. Images were obtained using a Leica TCS Sp8 X confocal microscope.

For both tested cell types, we were able to detect viral components in actin-containing nanotubes (Fig. 4). Shorter nanotubes were more prevalent in uninfected cells, while the long ones were found more frequently in infected cells, which could suggest that viral infection stimulates TNT formation.

To investigate the influence of viral infection on TNT formation, we compared the number and length of nanotubes formed by BoHV-1-infected cells and uninfected cells. TNT connections in a field of view (10 fields per experiment) were counted and measured using Lucia software in 6 separate experiments. A significant increase in the number of TNT connections was found between cells infected with BoHV-1 and uninfected cells. The increase was slightly higher in bovine fibroblasts (60%) than in KOP cells (~50%) (Fig. 5A). We also observed that BoHV-1 infection altered the ratio of short to long connections: in uninfected KOP cells long nanotubes (over 20 μm) constituted about 6% of all intercellular connections, while in BoHV-1-infected cells their percentage rose to 21%. In bovine fibroblasts the difference was even more

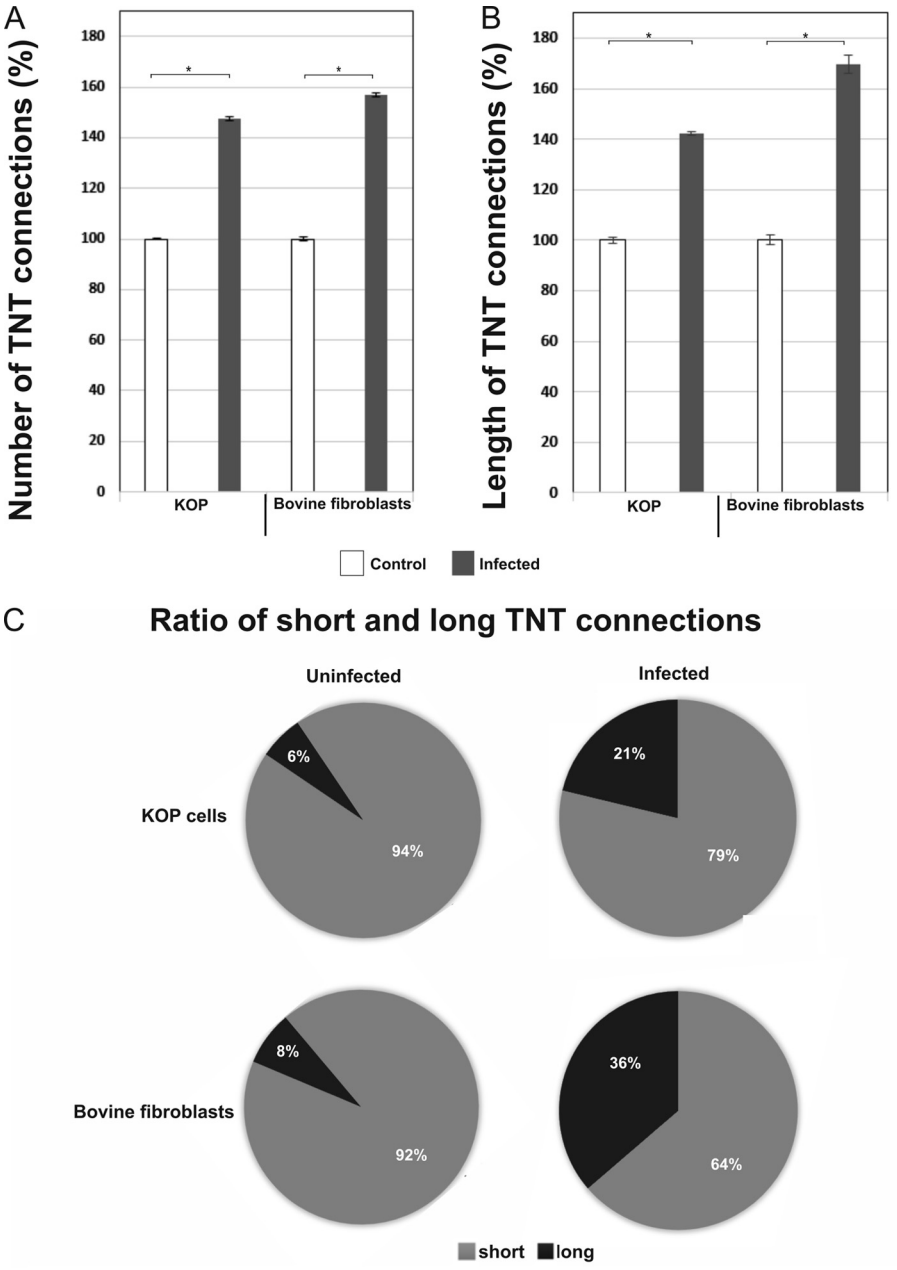

FIG 5 BoHV-1 infection increases the number and length of TNT connections. KOP cells and bovine fibroblasts were grown for 1 day on gelatin-coated coverslips and infected with BoHV-1-WT at an MOI of 1. Control cells were left uninfected. At 18 h.p.i., cells were fixed and stained with Alexa Fluor 488-phalloidin conjugate to visualize the actin cytoskeleton. The number and length of cell connections were quantified using confocal microscopy. TNT connections between infected and uninfected cells were manually counted and measured in 6 separate experiments. Data were collected using the Lucia program. (A) Comparison of the frequency of nanotubes formation in BoHV-1-infected and in uninfected cells. (B) Comparison of TNT length. (C) Analysis of ratio of short ($\leq$20 μm) to long ($>$20 μm) TNTs showed a significant shift toward long connections upon BoHV-1 infection. Data collected in 6 separate experiments represent the means, normalized to the value for control (uninfected) cells, arbitrarily set at 100%. *, $P < 0.01$.

evident: the number of long TNTs increased ~4.5 times (from 8% to 36%) after 18 h of infection with BoHV-1 (Fig. 5C). The increase in the length of nanotubes formed by infected KOP cells was around 40%, while in bovine fibroblasts it was significantly higher (70%) (Fig. 5B).

We also observed multiple projections tethering neighbor cells and forming cellular networks. Viral proteins were present inside cell bodies and both inside and on the

surface of tunneling nanotubes. They also accumulated in bubble-like structures along the nanotubes. The formation of such vesicles (named "gondolas") has been reported to potentially result from the transfer of a cargo that is too large to fit within the diameter of the tube (39).

To understand the transmission of viral components via intercellular connections in greater detail, we investigated the transfer of three individual BoHV-1 proteins that are the components of different parts of the viral particle. Glycoprotein E is an envelope component that, together with glycoprotein I, mediates the cell-to-cell spread of alphaherpesviruses. Capsid component VP26 is the smallest capsid protein and can be easily fused to a fluorescent tag to produce strong fluorescence emission and allow visualization of the movement of individual capsids. The tegument protein Us3 is a serine-threonine kinase involved in modulation of the host cell environment, e.g., by rearrangement of the cytoskeleton. We generated BoHV-1 mutants expressing enhanced green fluorescent protein fused either to the C terminus of gE (gE-GFP) or to the capsid protein VP26 (VP26-GFP). After infection of bovine cells with these mutants, fluorescent viral proteins were tracked in live or fixed cells. Additionally, Us3 was detected by immunofluorescence, and all cells were stained for the presence of F-actin.

All three viral proteins were visualized in infected cell bodies and in nanotubes (Fig. 6). Each of the investigated proteins was present both inside the "tunnels" and on their surface. Glycoprotein E (and Us3 protein) was often accumulated in vesicles traveling along the nanotube, which was usually not observed for capsids. These observations confirmed that different parts of the virion were transported by intercellular nanotubes. The next set of experiments was designed to verify whether the infectious BoHV-1 particles could move via these cellular extensions from one cell to another and use them as a route for direct transmission.

Tunneling nanotubes are involved in BoHV-1 cell-to-cell transmission. When the fluorescent signal emitted by viral proteins is traced by confocal microscopy, it is not clear whether the signal is derived from separate parts of the virion, individual protein aggregates, or whole viral particles. To address this issue, we analyzed the spread of BoHV-1 in the presence of neutralizing antibodies. BoHV-1, like other herpesviruses, can disseminate through two routes of transmission: cell-free entry and direct cell-to-cell spread. Cell-to-cell transmission can occur between cells that either are in close contact with each other or are connected by cell projections. The presence of neutralizing antibodies in the medium prevents virus-free entry, ensuring that viral transfer occurs only via the direct transmission route. We performed a standard virus neutralizing assay to determine the concentration of neutralizing antibody (anti-BoHV-1 serum) required to block virus-free entry. After determination of the optimal neutralization conditions, two populations of cells were prepared. The donor cells were infected with fluorescent BoHV-1 mutant (VP26-GFP) at a multiplicity of infection (MOI) of 1 for 1 h. After removal of unadsorbed virus, the cells were mixed at a 1:1 ratio with the uninfected (target) cells. The target cells were stained with red dye, Vybrant DiL, a lipophilic membrane stain that when incorporated into membranes produces orange-red fluorescence that allows one to easily distinguish target cells from infected cells in mixed cell cultures. The cells were seeded on gelatin-covered coverslips and cocultured in medium containing neutralizing serum to block free entry of the virus. The cells were monitored by confocal imaging for 18 h until the cells started to lyse. The experiments were performed with both types of cells used in this study: KOP cells and bovine fibroblasts. We observed the formation of long connections between uninfected target cells (red) and donor cells infected with green fluorescent virus. Cells in different stages of infection were visualized during these observations (Fig. 7). Donor cells showed signs of late stages of infection when green capsids were released from the nuclei and presumably incorporated into newly assembled viral particles. These cells were loaded with green signal, and numerous GFP-tagged particles were moving inside the intercellular nanotubes. Red target cells connected with donor cells clearly showed signs of active viral infection: green viral capsids accumulating inside the cell nucleus and

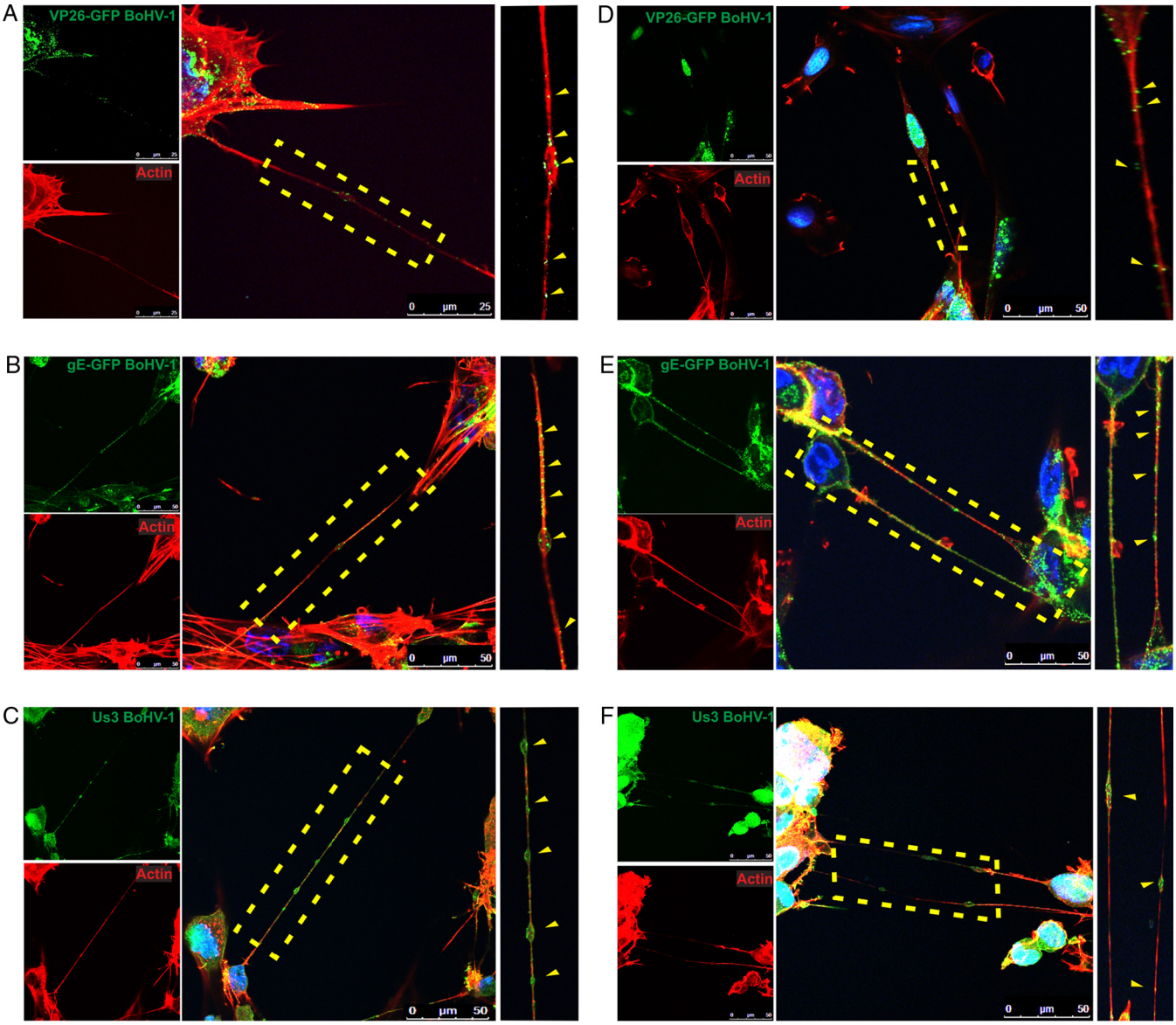

FIG 6 Viral proteins of BoHV-1 in tunneling nanotubes. KOP cells (A to C) and bovine fibroblasts (D to F) were infected at an MOI of 1 with BoHV-1-VP26-GFP for detection of GFP-tagged capsid protein VP26 (A and D), BoHV-1-gE-GFP for detection of GFP-tagged glycoprotein E (B and E), and BoHV-1-WT for detection of tegument protein US3 (C and F). At 12 h.p.i., the cells were fixed and additionally stained for F-actin (red) and nuclei (blue). Zoomed images of nanotubes (boxed regions) are in the right column. Yellow arrowheads indicate positions of viral proteins in nanotubes. Images were obtained using a Leica TCS Sp8 X confocal microscope.

intracytoplasmic capsids undergoing secondary envelopment near the nucleus. In cells with early-stage infection, single green capsids were visible in the nuclei. Moreover, the formation of virus-transferring intercellular connections was detected not only between cells of the same type but also between cocultured KOP cells and fibroblasts (Fig. 7C and D). In this experiment, KOP cells infected with green virus were cocultured with DiL-stained fibroblasts. We recorded transfer of GFP-labeled viral particles through a nanotube from an infected bovine fibroblast toward an uninfected KOP cell. Selected frames from this movie (Fig. 7D) show movements of green capsids inside the nanotube and, gradually, the start of productive infection in the nucleus of the connected DiL-stained KOP cell. At the end of the recording the nucleus of the donor cell is shown filled with green capsids which confirmed the active infection (see also Movie S3).

The transfer of GFP-labeled virus between epithelial cells and fibroblasts showed that transmission via TNTs may occur between various types of cells. These observa-

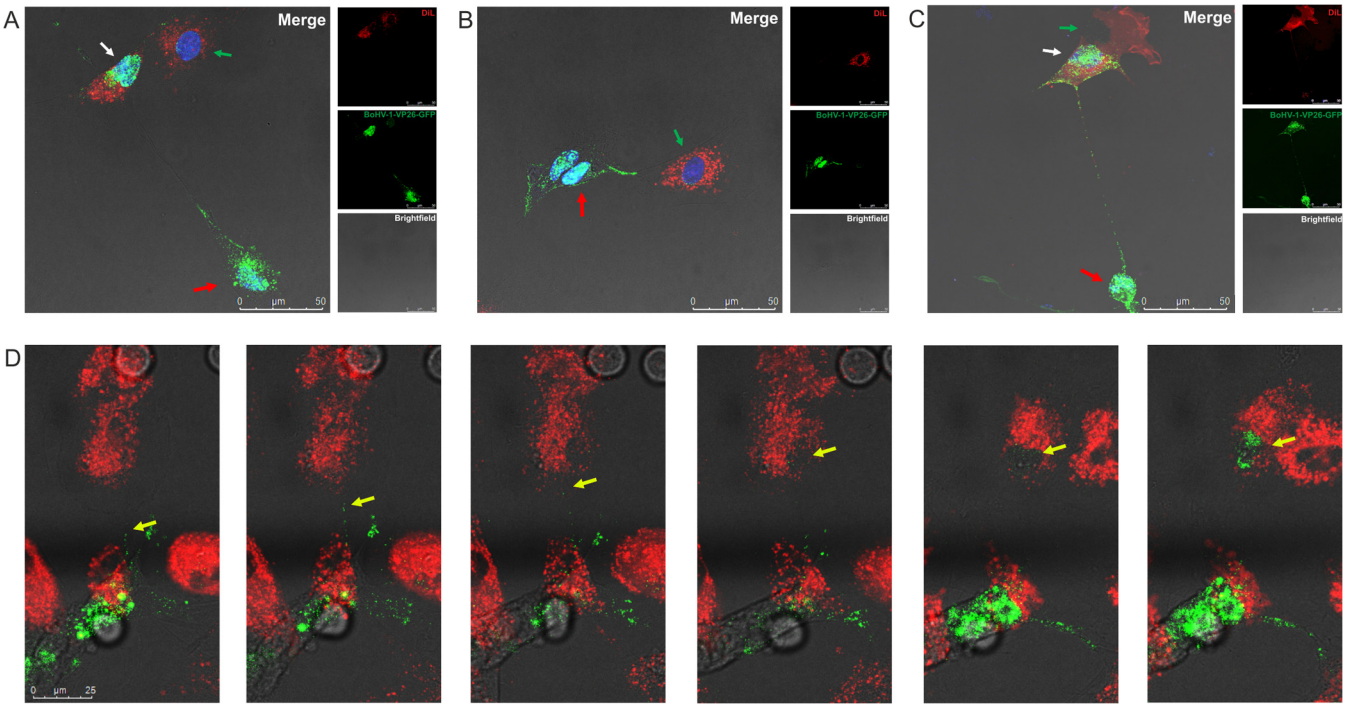

FIG 7 BoHV-1 cell-to-cell spread between two populations of cells through tunneling nanotubes in the presence of neutralizing antibodies. Red, uninfected (target) cells stained with DiL; green, donor cells infected with fluorescent mutant BoHV-1-VP26-GFP (green). Results for KOP cells (A), bovine fibroblasts (B), and cocultured KOP cells and fibroblasts (C and D) are shown. Green capsid proteins in the nuclei of target cells indicate the start of active infection. Red arrows indicate donor cells, the white arrows indicate more advanced infection in a target cell, and green arrows show single capsids in the nuclei of newly infected cells. Panel D shows selected images (see also Movie S3) from the recording showing steps in virus transfer from infected fibroblast to DIL-stained KOP cell. Yellow arrows indicate green capsids. The bright-field image shows the cell morphology. The cell nuclei were stained with DAPI (blue staining). Images were obtained using a Leica TCS Sp8 X confocal microscope.

tions indicated that infectious viral particles were transferred from donor to uninfected cells via membrane nanotubes despite the presence of neutralizing antibodies. These results support the notion that nanotubes allowing plasma continuity could be involved in the direct transmission of BoHV-1.

Further investigation of BoHV-1 transmission was conducted by observations of living cells infected with dually fluorescent BoHV-1. To obtain two-color BoHV-1 viral particles, the mCherry-tagged VP26 gene was introduced into the genome of gE-GFP recombinant BoHV-1. The resulting mutant (BoHV-1-gE-GFP-VP26-mCherry; red capsid and green envelope) was used to infect KOP cells and bovine fibroblasts seeded on glass bottom dishes. After infection, the experiment was performed in the presence of virus-neutralizing serum.

Beginning at 12 h.p.i. (for fibroblasts) or at 24 h.p.i. (for slowly growing KOP cells), live-cell movies were filmed for the subsequent 10 h to track the transfer of viral fluorescent proteins. Images were collected every 10 to 19 s, analyzed, and processed. Approximately 400 frames were combined into a movie illustrating viral transport inside nanotubes (see also Movies S4 and S5; the details of the recording are given in the legends to movies in the supplemental material).

In both cell types, we observed very dynamic movements of signal emitted by viral proteins in the intracellular environment and inside intercellular connections. In some cells, the GFP-gE-derived green signal accumulated in the perinuclear area, while red fluorescent capsids were still enclosed in nuclei (Movie S4, early stage of infection). In cells in more advanced stages of infection, the presence of a merged yellow signal indicated the maturation of enveloped viral particles (Movie S5, more advanced infection). In all stages of infection, rapid transfer of viral materials through the long nanotubes was consistently tracked, and we continuously observed the infection spread from infected to uninfected cells. The transfer seemed to be mostly unidirec-

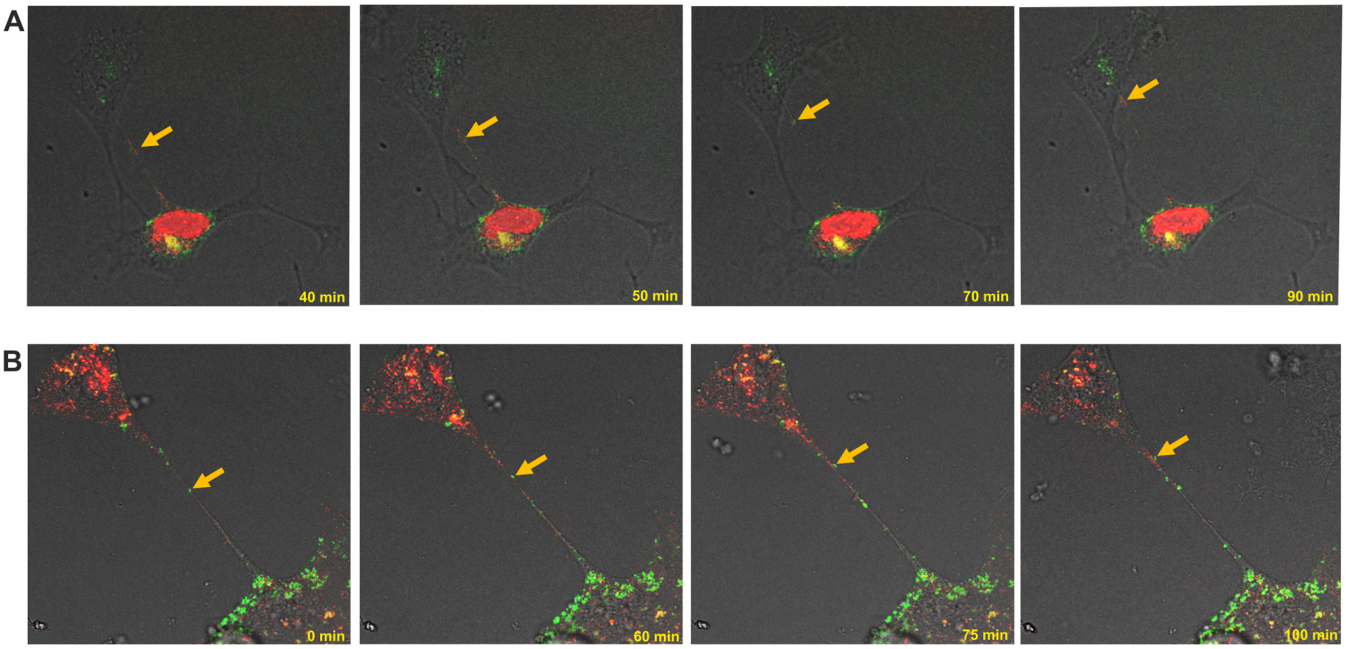

FIG 8 Cell-to-cell transfer of dually fluorescent BoHV-1 mutant through tunneling nanotubes in the presence of neutralizing antibodies. KOP cells (A) and bovine fibroblasts (B) were infected with dual-color fluorescent mutant BoHV-1-gE-GFP-VP26-mCherry. Red, viral capsids; green, envelope glycoprotein E. Selected images from live microscopy recordings show fluorescently tagged structures moving inside the tunneling nanotubes (indicated by yellow arrows) from infected to uninfected cells (see also Movies S4 and S5). Images and time-lapse movies were obtained using a Leica TCS Sp8 X confocal microscope.

tional, with occasional particles moving back and forth inside the connection. Selected frames from the live movies are presented in Fig. 8.

DISCUSSION

Herpesviruses can infect many types of cells and tissues, and the hallmark of herpesvirus infection is latency, the ability to remain in an infected host in a "hidden" form and to reactivate. This lifestyle requires the virus to be transmitted from the site of initial infection to the latency site, e.g., from epithelial to neuronal cells (in the case of alphaherpesviruses). Moreover, successful spread in the infected host is probably linked to the ability to infect other cell types and to exploit all pathways of cell communication (34). The entry of herpesviruses into cells is a multistep process that requires interactions between specific receptors and a number of viral glycoproteins that mediate initial attachment to cell surface heparan sulfate followed by fusion with the plasma membrane or by the endocytic pathway (40). However, like some other enveloped viruses, herpesviruses can also spread by direct cell-to-cell transmission from infected to uninfected cells without release into the extracellular environment. This route allows the barriers of multistep receptor binding to be avoided and helps to protect viruses from the host immune response. There is growing evidence that for some human pathogens, such as HIV and human T cell leukemia virus type 1 (HTLV-1), cell-to-cell spread appears to be the main mode of dissemination, not only within the infected host but also between hosts (41–43). For herpesviruses, which use multiple strategies to spread, including transmission between cells via tight junctions, filopodia, and virological synapses, direct cell-to-cell spread is an important immune-evasive strategy contributing to the capacity of this virus to survive after reactivation, when the virus is confronted with immune defenses developed during the primary infection (44–46).

In the present study, we investigated the transmission of a member of the *Alphaherpesvirinae* family, bovine herpesvirus 1, which is closely related to and shares many biological features with the human pathogens HSV-1 and VZV. We demonstrated that various types of intercellular projections are utilized for the transfer of BoHV-1. The

studies presented here were focused on the involvement of a specific type of connection, thin long membrane protrusions named tunneling nanotubes (TNTs), in viral transfer. Our findings were mostly based on confocal microcopy analysis facilitated by the use of fluorescently labeled viral mutants. The two types of bovine cells chosen for this study, epithelial cells (KOP cells) and cells of mesenchymal origin (primary fibroblasts), are nontransformed cells with a limited life span and thus are more similar to natural tissues than typical laboratory cell lines. We showed that both cell types were able to form connections of variable lengths that could be classified as TNTs. We detected both actin filaments and tubulin in most TNTs. No major differences between nanotubes formed by fibroblasts and epithelial cells were observed, although many reports have shown that the morphology, dimensions, and composition of nanotubes formed by specific types of cells can vary (e.g., T cells and macrophages) (12). We observed the transfer of cellular components, including mitochondria and viral proteins, from one cell to another, which is consistent with the well documented role of TNTs in the exchange of various cargo between physically separated cells.

The question arises of whether and to what extent the nanotubes observed between infected cells were induced by virus infection. Several reports have demonstrated that viruses can induce TNT formation. HIV infection of human macrophage stimulates TNT formation in a manner correlated with virus replication (47). A significantly increased frequency of nanotube production has also been reported for cells infected with influenza virus (27, 48). As shown in this report, we detected TNT-like intercellular connections between both infected and uninfected cells used in this study. Some of these connections were relatively stable, but most of them were transient bridges, quickly disappearing or breaking. In virus-infected cells, nanotubes often formed networks that simultaneously connected several cells. Quantification of intercellular extensions showed a significant increase in the number of projections, particularly the long ones, in BoHV-1-infected cells compared to uninfected cells. BoHV-1 infection stimulated the appearance of long TNTs (over 20 μm and sometimes as long as 120 μm). This tendency was more clearly manifested in fibroblasts (where the ratio of long to short connections in BoHV-1-infected cells rose from 8% to 36%) than in epithelial (KOP) cells. These results indicate that the ability to form nanotubes is cell specific; this was also shown for HIV infection, where changes in the length of TNTs were not detected in HIV-infected macrophages (47). The increase in TNT production suggests that these projections can be exploited by the virus for more efficient spread and probably also *in vivo* during natural infection.

In this study, we used immunofluorescence to confirm the presence of BoHV-1 in long intercellular connections. Viral proteins were localized both inside and on the surface of nanotubes and in numerous vesicles loaded with viral materials. During infection of cultured cells with the BoHV-1 wild type or fluorescent mutants, we were able to track individual viral proteins in TNTs. For our observations, we selected proteins that are components of different structural parts of the herpesvirus virion: an envelope glycoprotein (gE), a tegument protein (Us3 kinase), and a capsid structural protein (VP26). All three proteins were visualized both in fixed and in live cells at various time points after infection, which confirmed that all substructures of the viral particles were transported, either individually or as parts of an assembled viral particle. They were visible either as individual puncta or as protein-loaded vesicles moving along nanotubes. Glycoprotein E and Us3 protein were more often visible in bubble-like vesicles (gondolas) than was capsid component VP26, which migrated mostly in the form of compact structures, probably assembled capsids. In our previous studies of gE-GFP expression, we often noticed that this glycoprotein was readily distributed to cell projections and often accumulated in bubble-like structures along cellular extensions formed not only by epithelial cells but also by neurons transfected with BoHV-1 gE (M. Panasiuk, A. Brzozowska, M. Rychlowski, J. Jaworski, and K. Bienkowska-Szewczyk, poster session presented at the 38th Annual International Herpesvirus Workshop, 20 to 24 July 2013, Grand Rapids, MI). Glycoprotein E is one of the main mediators of alphaherpesvirus cell-to-cell spread and has been shown to accumulate specifically in

cell junctions during viral infection (49, 50). No specific cellular factors interacting with gE during its function in viral direct transmission (apart from IDE for VZV) have been isolated to date (51). If such a factor exists and is identified, it would be interesting to determine whether it is somehow associated with the area of the TNT formation in infected cells.

Capsid movements were visualized with two virus mutants, BoHV-1 VP26-GFP (green capsid) and the dual-color BoHV-1-gE-GFP-VP26-mCherry mutant (red capsid and green envelope). For both types of mutants, we clearly observed the fluorescent capsids traveling through nanotubes to the uninfected cell. It has been postulated that during axonal transfer, unenveloped capsids and glycoproteins (loaded into vesicles) are transported separately and later reassembled into mature virions (52). This phenomenon might also function as a working hypothesis in the case of viral transport mediated by TNTs: while examining the dual-color mutant trafficking in live cells, we did not directly detect two-color structures inside TNTs (although that may have been the result of how the viral particle was positioned in the tube), and the two signals appeared to travel separately in the nanotubes. However, the presence of intact virions in nanotubes was reported for projections formed by pseudorabies virus (PRV)-infected cells (53).

In reports concerning the transfer of PRRSV (28) and influenza virus (29) via TNTs, the transfer of several structural proteins was also shown. It was not clear in such analyses whether the observed transfer reflected the transport of viral material together with other cytoplasmic cargo or the transmission of mature viral particles. In the case of RNA viruses, this question was addressed by searching for RNA or replication complexes in membrane nanotubes. We did not attempt to detect viral DNA or BoHV-1 replication-connected proteins in nanotubes, but our confocal imaging of living cells demonstrated that the transfer of fluorescent signal emitted by viral proteins from infected to uninfected cells resulted in the initiation of an active infection cycle in target cells, confirming the presence of infectious material in the viral cargo migrating via TNTs. Thus, we can safely assume that the capsids contained viral DNA. We used two approaches to confirm that TNTs were involved in the spread of BoHV-1 infection. All experiments were conducted in the presence of neutralizing serum, which completely blocked the entry of free virus. In the first assay, we examined infection of DiL-stained recipient cells cocultured with a population of donor cells infected with GFP-tagged capsid virus. In the second assay, the infection events were tracked with a dually fluorescent viral mutant. The dynamic trafficking of fluorescent structures—viral capsids or complete virions—was clearly visible during these observations. Although it was not always easy to determine whether the transfer of cargo via TNTs was bidirectional or unidirectional, the live movies allowed us to follow the movements of single capsids and mostly revealed a flow of viral structures from infected to uninfected cells. Inside the cells infected with the BoHV-1 dual-color mutant, we observed a green (gE) signal in the cytoplasmic perinuclear area and red capsids accumulating in the nucleus in the early stage of infection (Fig. 8). In target cells, the start of infection was manifested by the appearance of single capsids in the nucleus. In the later phase of infection, areas with a yellow signal appeared inside the cells, indicating the presence of enveloped viral particles. The formation of TNTs was also detected between two different types of cells used in this study. These connections effectively mediated virus transfer between epithelial cells and fibroblasts. Such transfer is likely to be involved in virus dissemination in the skin *in vivo*, but it remains to be confirmed whether it also occurs during natural infection. The transfer via TNT occurs probably in combination with other pathways of intercellular communication (other types of cell protrusions, exosomes, or gap junctions), and the preferred pathway may depend on cell condition. However, the fact that herpesvirus infection stimulates the formation of intercellular bridges and changes the ratio of short to long connections indicates that nanotubes play role in the dissemination of infection. All our observations confirmed that BoHV-1 transmission occurred when no cell-free infection was possible, and tunneling nanotubes were used as a pathway for direct cell-to-cell spread of the virus.

PRV studies have indicated for the first time that Us3 protein kinase, a protein that is highly conserved among herpesviruses, stimulates the formation of long intercellular projections (54). While this manuscript was being edited for submission, another report about the possible role of tunneling nanotubes in alphaherpesvirus infection was published (53). The authors demonstrated that cells infected with pseudorabies virus or transfected with PRV Us3 produced TNT-type projections involved in the transport of viral proteins and viral particles. They presented data showing that the activity of Us3 is crucial for the formation of PRV-induced nanotubes. In our previous studies concerning the functions of BoHV-1 Us3 kinase, we also observed that overexpression of BoHV-1 Us3 disrupted the actin cytoskeleton architecture and caused dynamic production of a network of long cell extensions (55). However, preliminary analyses of cells infected with BoHV-1 Us3 null mutant showed that such cells produce some projections, although more slowly and less intensively (data not shown). The TNTs induced by PRV Us3 were very stable, in contrast to our observations of the fragility of tunneling nanotubes formed between BoHV-1-infected cells. Despite some differences between individual herpesviruses, the PRV reports (53, 54) together with our data provide evidence that alphaherpesviruses trigger the formation of TNT and that these structures can be involved in virus intercellular spread.

Unlike filopodia, tunneling nanotubes are not attached to any substratum when forming a bridge between cells, and they "float" in the medium. Apart from this structural difference, it is not clear whether these structures have specialized functions in comparison to other cell projections. It is not known how materials transferred by TNTs are selected. It has recently been suggested (56) that filopodia and TNTs are formed through different molecular mechanisms associated with a "switch" in actin regulators. The ability to develop TNTs is a potential defense response to stress. Viral infection is also a stress factor that may trigger the formation of nanotube connections, and further investigations are needed to better understand the relationship between TNTs and viral pathogenesis.

MATERIALS AND METHODS

Cell cultures and viruses. MDBK (bovine kidney epithelial cells; ATCC) cells and the bovine KOP cell line (fetal bovine oropharynx cells; Friedrich-Loeffler Institute, Greifswald-Insel Riems, Germany) were grown in minimal essential medium (MEM; Sigma-Aldrich) supplemented with 10% fetal bovine serum (FBS) and penicillin-streptomycin solution. All cells were maintained at 37°C in a humidified 5% CO_2 atmosphere.

Bovine fibroblasts are a primary cell line isolated from skin excised from calf ear (International Institute of Molecular and Cellular Biology, Warsaw, Poland). The cells were maintained in Dulbecco's modified Eagle's medium with 4,500 mg glucose/liter (Sigma-Aldrich) supplemented with 10% fetal bovine serum and penicillin-streptomycin solution.

The Dutch BoHV-1.1 field strain Lam (BoHV-1-WT), mutant with GFP fused to capsid protein VP26 (BoHV-1-VP26-GFP), mutant with GFP fused to the C terminus of glycoprotein E (BoHV1-gE-GFP), and dual-color mutant with GFP fused to the C terminus of glycoprotein E and mCherry fused to capsid protein VP26 (BoHV-1-gE-GFP-VP26-mCherry) were propagated in primary bovine fibroblasts and stored at −70°C until use.

Antibodies and dyes. Goat anti-BoHV-1 serum (VMRD, Inc.) was used at a dilution of 1:1,000. Rabbit anti-BoHV-1-Us3 serum (a kind gift from Günther M. Keil, Friedrich Loeffler Institute, Greifswald-Insel Riems, Germany) was used at a 1:1,000 dilution. Mouse monoclonal anti-α-tubulin antibody (Sigma) was used at a 1:2,000 dilution. F-actin was stained with phalloidin-TRITC conjugate (Sigma) at a 1:2,000 dilution. Secondary goat anti-rabbit IgG Alexa Fluor 488 and rabbit anti-goat IgG Alexa Fluor 488 conjugates (Molecular Probes) were used at a 1:2,000 dilution. Vybrant DiL cell labeling solution (Molecular Probes) and MitoTracker Red (Molecular Probes) was used to label cells according to the supplier's instructions. Nuclear staining was performed with 4′,6-diamidino-2-phenylindole (DAPI) using ProLong Gold antifade mountant with DAPI (Invitrogen).

BoHV-1 mutant construction. All virus mutants constructed for this study were obtained by the cotransfection method. Cassette plasmids were cotransfected together with full-length BoHV-1 DNA or BoHV-1-gE-GFP DNA into KOP cells using calcium chloride transfection. After homologous recombination, the mutants were isolated by picking positive plaques.

BoHV-1-gE-GFP mutant. The enhanced green fluorescent protein (EGFP) gene was amplified by PCR using primers FOR (5′-AACCCTCCGCAAGGGCGAGGA-3′) and REV (5′-TGGCCTAGATCTATTGAGGACCCCT TCCAA-3′). The EGFP sequence was ligated into the EcoNI recognition site in the gE 760-bp fragment sequence in the pMR plasmid. The gE-EGFP fragment was introduced into the pUC318 plasmid encompassing the complete gE open reading frame (ORF). The full-length modified gE-EGFP sequence was subsequently cloned into the pUS plasmid to generate the pUSgEGFP cassette plasmid, which was

cotransfected with the full-length BoHV-1 DNA into KOP cells. The mutant was isolated and purified from a single green fluorescent plaque.

BoHV-1-gE-GFP-VP26-mCherry mutant. BoHV-1 DNA sequences flanking the open reading frame of the UL35 gene (coding for VP26 protein) were amplified in two separate PCRs with primer pair 36 FOR (5′-ATTATAGAATTCTCTGCGCTGTCGGGCCTTGGCTC-3′) and 35 REV (5′-TTATACCATGCATACCGGTGCCGG GATCGACCGAT-3′) or 35 FOR (5′-ATTATAGCATGCATGGCGTCGTCGAACCGCGAGTG-3′) and 34 REV (5′-ATTATAGGATCCTTTGGCCTTTTCGGCGCGCCTGG-3′). Both amplification products were cloned and combined in the pJET vector, such that the AgeI and NsiI recognition sites were introduced at the 5′ terminus of the UL35 gene, resulting in pJET 36/34. The mCherry gene was amplified by PCR using the primer pair FOR (5′-CACCATGCATAGCAAGGGCGAGGAGGATAAC-3′) and REV (5′-ATTACCGGTCTTGTACAGCTCGTCC ATGCC-3′). The mCherry sequence was ligated into pJET 36/34 at NsiI and AgeI sites to generate the pJET VP26-mCherry cassette plasmid. The cassette plasmid was cotransfected with full-length BoHV-1-gE-GFP DNA into KOP cells. The mutant was isolated and purified from doubly fluorescent (red and green) plaques.

The BoHV-1-VP26-GFP mutant with GFP fused to capsid protein VP26 was constructed as described previously (57).

Immunofluorescence analysis. (i) Analysis of the cytoskeleton composition. KOP cells and bovine fibroblasts were grown on gelatin-coated coverslips (Sigma-Aldrich). At 24 h after seeding, the cells were fixed by adding 16% PFA (Alfa Aesar) directly to the medium to a final concentration of 4% PFA. The cells were incubated for 2 h at 8°C and air dried. Next, the cells were permeabilized with 0.2% Triton X-100 in phosphate-buffered saline (PBS) for 5 min and washed 3 times with PBS. After incubation with primary antibody for 1 h, the cells were washed 3 times with PBS, and the respective secondary antibody was added for 1 h. The antibody solutions were prepared in PBS plus 5% FBS. Coverslips were mounted using ProLong Gold antifade mountant with DAPI (Invitrogen), and the cells were analyzed using a Leica TCS Sp8 X confocal microscope.

(ii) Analysis of infected cells. KOP cells and bovine fibroblasts were grown on gelatin-coated coverslips (Sigma-Aldrich) for 1 day prior to infection. The cells were infected with BoHV-1 at an MOI of 1 for 1 h at 37°C to allow virus adsorption. Next, the virus inoculum was removed, cells were washed, and fresh medium was added. At 12 h.p.i., the cells were fixed by adding 16% PFA (Alfa Aesar) directly to medium to a final concentration of 4% PFA. The cells were incubated for 2 h at 8°C and air dried. Next, cells were permeabilized with 0.2% Triton X-100 in PBS for 5 min and washed 3 times with PBS. Primary antibody was added for 1 h, the cells were washed 3 times with PBS, and the respective secondary antibody was added for 1 h. Antibody solutions were prepared in PBS plus 5% FBS. Coverslips were mounted using ProLong Gold antifade mountant with DAPI (Invitrogen). Cells were analyzed using a Leica TCS Sp8 X confocal microscope.

Coculture assay. To analyze BoHV-1 transmission in the presence of neutralizing serum to block free-cell transmission, a two-color population model was prepared. To distinguish between naive and infected cells, the target cells were stained with Vybrant DiL cell-labeling solution (Molecular Probes) according to the supplier's protocol. The donor cells were infected with the fluorescent BoHV-1 mutant (BoHV-1-VP26-GFP) at an MOI of 1. The cells were incubated with virus for 1 h at 37°C to allow virus adsorption, washed, and mixed with target cells at a 1:1 ratio. The cells were seeded on gelatin-coated coverslips (Sigma-Aldrich) and cocultured in medium containing neutralizing anti-BoHV1 serum at a concentration that blocked cell-free spread of the virus (the amount of antibodies was determined in a standard neutralization assay as described below). The same procedure was used for KOP cells and bovine fibroblasts. At 18 h.p.i., the cells were fixed by adding 16% PFA (Alfa Aesar) directly to the medium to a final concentration of 4% PFA. The cells were incubated for 2 h at 8°C and air dried. Coverslips were mounted using ProLong Gold antifade mountant with DAPI (Invitrogen), and the cells were examined using a Leica TCS Sp8 X confocal microscope.

Neutralization assay. Goat anti-BoHV-1 serum (VMRD, Inc.) was used in a standard BoHV-1 neutralization assay. A 2-fold series of dilutions of the serum sample were prepared in a 96-well plate (100 μl/well). Samples of BoHV-1-gE-GFP fluorescent mutant lysate were added to individual wells and mixed with the serum dilutions. The mixture was incubated for 1 h at 37°C. After incubation, the serum-virus complex was transferred onto confluent monolayers of KOP cells. At 24 h.p.i., the cells were analyzed using a fluorescence microscope for GFP-positive cells. The serum dilution that caused 100% inhibition of virus infection was used in subsequent experiments to block cell-free entry of the virus.

Confocal live-cell imaging analysis. Time-lapse imaging analysis was performed using a Leica TCS Sp8 X confocal microscope equipped with an environmental chamber at 37°C and 5% CO_2. Images were obtained at a magnification of $\times$63. The relative time and scale bar are shown in the bottom of each movie. KOP cells and bovine fibroblasts were seeded on glass bottom dishes (Willco Wells) 1 day prior to infection. The cells were infected with BoHV-1-VP26-GFP or the dual-color BoHV-1-gE-GFP-VP26-mCherry virus mutant at a low MOI to enable observations of single infected cells. After 1 h of adsorption at 37°C, the virus inoculum was replaced with fresh medium containing neutralizing serum at the concentration determined in the neutralization assay. The cells were analyzed for 10 h, and images were collected every 10 to 19 s. The collected images were processed using Leica Software LasX and CorelDRAW X7. Representative fragments of recordings are shown as Movies S3, S4, and S5 in the supplemental material.

Statistics. Statistical differences were calculated on the raw data by two-tailed Student's *t* test using Mann-Whitney U Test Calculator (free software available at http://www.socscistatistics.com); a *P* value of <0.01 was considered statistically significant.

SUPPLEMENTAL MATERIAL

Supplemental material for this article may be found at https://doi.org/10.1128/JVI.00090-18.

SUPPLEMENTAL FILE 1, MP4 file, 3.7 MB.
SUPPLEMENTAL FILE 2, MP4 file, 3.2 MB.
SUPPLEMENTAL FILE 3, MP4 file, 8.0 MB.
SUPPLEMENTAL FILE 4, MP4 file, 2.6 MB.
SUPPLEMENTAL FILE 5, MP4 file, 4.3 MB.
SUPPLEMENTAL FILE 6, PDF file, 0.2 MB.

ACKNOWLEDGMENTS

We thank Jacek Jaworski and Ewa Liszewska from the International Institute of Molecular and Cellular Biology in Warsaw, Poland, for performing the bovine fibroblast isolation, Günther M. Keil from Friedrich Loeffler Institute, Greifswald-Insel Riems, Germany, for the anti-Us3 BoHV-1 serum, and Kurt Tobler from the University of Zurich for the BoHV-1-VP26-GFP mutant.

This work was supported by the National Science Center, Poland (grant 2012/04/A/NZ1/00056 to K. Bieńkowska-Szewczyk).

REFERENCES

1. Kumar NM, Gilula NB. 1996. The gap junction communication channel. Cell 84:381–388. https://doi.org/10.1016/S0092-8674(00)81282-9.
2. Sattentau Q. 2008. Avoiding the void: cell-to-cell spread of human viruses. Nat Rev Microbiol 6:815–826. https://doi.org/10.1038/nrmicro1972.
3. Gurke S, Barroso JF, Gerdes HH. 2008. The art of cellular communication: tunneling nanotubes bridge the divide. Histochem Cell Biol 129:539–550. https://doi.org/10.1007/s00418-008-0412-0.
4. Rustom A, Saffrich R, Markovic I, Walther P, Gerdes HH. 2004. Nanotubular highways for intercellular organelle transport. Science 303:1007–1010. https://doi.org/10.1126/science.1093133.
5. Sherer NM, Lehmann MJ, Jimenez-Soto LF, Horensavitz C, Pypaert M, Mothes W. 2007. Retroviruses can establish filopodial bridges for efficient cell-to-cell transmission. Nat Cell Biol 9:310–315. https://doi.org/10.1038/ncb1544.
6. Wang X, Veruki ML, Bukoreshtliev NV, Hartveit E, Gerdes HH. 2010. Animal cells connected by nanotubes can be electrically coupled through interposed gap-junction channels. Proc Natl Acad Sci U S A 107:17194–17199. https://doi.org/10.1073/pnas.1006785107.
7. Hase K, Kimura S, Takatsu H, Ohmae M, Kawano S, Kitamura H, Ito M, Watarai H, Hazelett CC, Yeaman C, Ohno H. 2009. M-Sec promotes membrane nanotube formation by interacting with Ral and the exocyst complex. Nat Cell Biol 11:1427–1432. https://doi.org/10.1038/ncb1990.
8. Zhu D, Tan KS, Zhang X, Sun AY, Sun GY, Lee JC. 2005. Hydrogen peroxide alters membrane and cytoskeleton properties and increases intercellular connections in astrocytes. J Cell Sci 118:3695–3703. https://doi.org/10.1242/jcs.02507.
9. Wang X, Bukoreshtliev NV, Gerdes HH. 2012. Developing neurons form transient nanotubes facilitating electrical coupling and calcium signaling with distant astrocytes. PLoS One 7:e47429. https://doi.org/10.1371/journal.pone.0047429.
10. Austefjord MW, Gerdes HH, Wang X. 2014. Tunneling nanotubes: diversity in morphology and structure. Commun Integr Biol 7:e27934. https://doi.org/10.4161/cib.27934.
11. Onfelt B, Nedvetzki S, Yanagi K, Davis DM. 2004. Cutting edge: membrane nanotubes connect immune cells. J Immunol 173:1511–1513. https://doi.org/10.4049/jimmunol.173.3.1511.
12. Onfelt B, Nedvetzki S, Benninger RK, Purbhoo MA, Sowinski S, Hume AN, Seabra MC, Neil MA, French PM, Davis DM. 2006. Structurally distinct membrane nanotubes between human macrophages support long-distance vesicular traffic or surfing of bacteria. J Immunol 177:8476–8483. https://doi.org/10.4049/jimmunol.177.12.8476.
13. Miller J, Fraser SE, McClay D. 1995. Dynamics of thin filopodia during sea urchin gastrulation. Development 121:2501–2511.
14. Chinnery HR, Pearlman E, McMenamin PG. 2008. Cutting edge: membrane nanotubes *in vivo*: a feature of MHC class II+ cells in the mouse cornea. J Immunol 180:5779–5783. https://doi.org/10.4049/jimmunol.180.9.5779.
15. Seyed-Razavi Y, Hickey MJ, Kuffová L, McMenamin PG, Chinnery HR. 2013. Membrane nanotubes in myeloid cells in the adult mouse cornea represent a novel mode of immune cell interaction. Immunol Cell Biol 91:89–95. https://doi.org/10.1038/icb.2012.52.
16. McKinney MC, Kulesa PM. 2011. In vivo calcium dynamics during neural crest cell migration and patterning using GCaMP3. Dev Biol 358:309–317. https://doi.org/10.1016/j.ydbio.2011.08.004.
17. Sisakhtnezhad S, Khosravi L. 2015. Emerging physiological and pathological implications of tunneling nanotubes formation between cells. Eur J Cell Biol 94:429–443. https://doi.org/10.1016/j.ejcb.2015.06.010.
18. Kimura S, Hase K, Ohno H. 2013. The molecular basis of induction and formation of tunneling nanotubes. Cell Tissue Res 352:67–76. https://doi.org/10.1007/s00441-012-1518-1.
19. Lou E, Fujisawa S, Morozov A, Barlas A, Romin Y, Dogan Y, Gholami S, Moreira AL, Manova-Todorova K, Moore MA. 2012. Tunneling nanotubes provide a unique conduit for intercellular transfer of cellular contents in human malignant pleural mesothelioma. PLoS One 7:e33093. https://doi.org/10.1371/journal.pone.0033093.
20. Zhu S, Victoria GS, Marzo L, Ghosh R, Zurzolo C. 2015. Prion aggregates transfer through tunneling nanotubes in endocytic vesicles. Prion 9:125–135. https://doi.org/10.1080/19336896.2015.1025189.
21. Gousset K, Schiff E, Langevin C, Marijanovic Z, Caputo A, Browman DT, Chenouard N, de Chaumont F, Martino A, Enninga J, Olivo-Marin JC, Männel D, Zurzolo C. 2009. Prions hijack tunnelling nanotubes for intercellular spread. Nat Cell Biol 11:328–336. https://doi.org/10.1038/ncb1841.
22. Sowinski S, Jolly C, Berninghausen O, Purbhoo MA, Chauveau A, Köhler K, Oddos S, Eissmann P, Brodsky FM, Hopkins C, Onfelt B, Sattentau Q, Davis DM. 2008. Membrane nanotubes physically connect T cells over long distances presenting a novel route for HIV-1 transmission. Nat Cell Biol 10:211–219. https://doi.org/10.1038/ncb1682.
23. Sowinski S, Alakoskela JM, Jolly C, Davis DM. 2011. Optimized methods for imaging membrane nanotubes between T cells and trafficking of HIV-1. Methods 53:27–33. https://doi.org/10.1016/j.ymeth.2010.04.002.
24. Murooka TT, Deruaz M, Marangoni F, Vrbanac VD, Seung E, von Andrian UH, Tager AM, Luster AD, Mempel TR. 2012. HIV-infected T cells are migratory vehicles for viral dissemination. Nature 490:283–287. https://doi.org/10.1038/nature11398.
25. Malik S, Eugenin EA. 2016. Mechanisms of HIV neuropathogenesis: role of cellular communication systems. Curr HIV Res 14:400–411. https://doi.org/10.2174/1570162X14666160324124558.
26. Hashimoto M, Bhuyan F, Hiyoshi M, Noyori O, Nasser H, Miyazaki M, Saito T, Kondoh Y, Osada H, Kimura S, Hase K, Ohno H, Suzu S. 2016. Potential role of the formation of tunneling nanotubes in HIV-1 spread in macro-

phages. J Immunol 196:1832–1841. https://doi.org/10.4049/jimmunol.1500845.
27. Roberts KL, Manicassamy B, Lamb RA. 2015. Influenza A virus uses intercellular connections to spread to neighboring cells. J Virol 89:1537–1549. https://doi.org/10.1128/JVI.03306-14.
28. Guo R, Katz BB, Tomich JM, Gallagher T, Fang Y. 2016. Porcine reproductive and respiratory syndrome virus utilizes nanotubes for intercellular spread. J Virol 90:5163–5175. https://doi.org/10.1128/JVI.00036-16.
29. Abendroth A, Kinchington PR, Slobedman B. 2010. Varicella zoster virus immune evasion strategies. Curr Top Microbiol Immunol 342:155–171.
30. Melchjorsen J, Matikainen S, Paludan SR. 2009. Activation and evasion of innate antiviral immunity by herpes simplex virus. Viruses 1:737–759. https://doi.org/10.3390/v1030737.
31. Friedman HM. 2003. Immune evasion by herpes simplex virus type 1, strategies for virus survival. Trans Am Clin Climatol Assoc 114:103–112.
32. Enquist LW, Tomishima MJ, Gross S, Smith GA. 2002. Directional spread of an alpha-herpesvirus in the nervous system. Vet Microbiol 86:5–16. https://doi.org/10.1016/S0378-1135(01)00486-2.
33. Smith GA, Gross SP, Enquist LW. 2001. Herpesviruses use bidirectional fast-axonal transport to spread in sensory neurons. Proc Natl Acad Sci U S A 98:3466–3470. https://doi.org/10.1073/pnas.061029798.
34. Karasneh GA, Shukla D. 2011. Herpes simplex virus infects most cell types in vitro: clues to its success. Virol J 8:481. https://doi.org/10.1186/1743-422X-8-481.
35. Muylkens B, Thiry J, Kirten P, Schynts F, Thiry E. 2007. Bovine herpesvirus 1 infection and infectious bovine rhinotracheitis. Vet Res 38:181–209. https://doi.org/10.1051/vetres:2006059.
36. Tyborowska J, Bieńkowska-Szewczyk K, Rychłowski M, Van Oirschot JT, Rijsewijk FA. 2000. The extracellular part of glycoprotein E of bovine herpesvirus 1 is sufficient for complex formation with glycoprotein I but not for cell-to-cell spread. Arch Virol 145:333–351. https://doi.org/10.1007/s007050050026.
37. Verweij MC, Lipinska AD, Koppers-Lalic D, van Leeuwen WF, Cohen JI, Kinchington PR, Messaoudi I, Bienkowska-Szewczyk K, Ressing ME, Rijsewijk FA, Wiertz EJ. 2011. The capacity of UL49.5 proteins to inhibit TAP is widely distributed among members of the genus *Varicellovirus*. J Virol 85:2351–2363. https://doi.org/10.1128/JVI.01621-10.
38. Cuddington BP, Mossman KL. 2014. Permissiveness of human cancer cells to oncolytic bovine herpesvirus 1 is mediated in part by KRAS activity. J Virol 88:6885–6895. https://doi.org/10.1128/JVI.00849-14.
39. Hurtig J, Chiu DT, Onfelt B. 2010. Intercellular nanotubes: insights from imaging studies and beyond. Wiley Interdiscip Rev Nanomed Nanobiotechnol 2:260–276. https://doi.org/10.1002/wnan.80.
40. Agelidis AM, Shukla D. 2015. Cell entry mechanisms of HSV: what we have learned in recent years. Future Virol 10:1145–1154. https://doi.org/10.2217/fvl.15.85.
41. Mothes W, Sherer NM, Jin J, Zhong P. 2010. Virus cell-to-cell transmission. J Virol 84:8360–8368. https://doi.org/10.1128/JVI.00443-10.
42. Dutartre H, Clavière M, Journo C, Mahieux R. 2016. Cell-free versus cell-to-cell infection by human immunodeficiency virus type 1 and human T-lymphotropic virus type 1: exploring the link among viral source, viral trafficking, and viral replication. J Virol 90:7607–7617. https://doi.org/10.1128/JVI.00407-16.
43. Gross C, Thoma-Kress AK. 2016. Molecular mechanisms of HTLV-1 cell-to-cell transmission. Viruses 8:74. https://doi.org/10.3390/v8030074.
44. Curanovic D, Enquist LW. 2009. Directional transneuronal spread of α-herpesvirus infection. Future Virol 4:591. https://doi.org/10.2217/fvl.09.62.
45. Chang K, Baginski J, Hassan SF, Volin M, Shukla D, Tiwari V. 2016. Filopodia and viruses: an analysis of membrane processes in entry mechanisms. Front Microbiol 7:300. https://doi.org/10.3389/fmicb.2016.00300.
46. Aubert M, Yoon M, Sloan DD, Spear PG, Jerome KR. 2009. The virological synapse facilitates herpes simplex virus entry into T cells. J Virol 83:6171–6183. https://doi.org/10.1128/JVI.02163-08.
47. Eugenin EA, Gaskill PJ, Berman JW. 2009. Tunneling nanotubes (TNT) are induced by HIV-infection of macrophages: a potential mechanism for intercellular HIV trafficking. Cell Immunol 254:142–148. https://doi.org/10.1016/j.cellimm.2008.08.005.
48. Kumar A, Kim JH, Ranjan P, Metcalfe MG, Cao W, Mishina M, Gangappa S, Guo Z, Boyden ES, Zaki S, York I, García-Sastre A, Shaw M, Sambhara S. 2017. Influenza virus exploits tunneling nanotubes for cell-to-cell spread. Sci Rep 7:40360. https://doi.org/10.1038/srep40360.
49. Dingwell KS, Brunetti CR, Hendricks RL, Tang Q, Tang M, Rainbow AJ, Johnson DC. 1994. Herpes simplex virus glycoproteins E and I facilitate cell-to-cell spread in vivo and across junctions of cultured cells. J Virol 68:834–845.
50. Mo C, Schneeberger EE, Arvin AM. 2000. Glycoprotein E of varicella-zoster virus enhances cell-cell contact in polarized epithelial cells. J Virol 74:11377–11387. https://doi.org/10.1128/JVI.74.23.11377-11387.2000.
51. Li Q, Ali MA, Cohen JI. 2006. Insulin degrading enzyme is a cellular receptor mediating varicella-zoster virus infection and cell-to-cell spread. Cell 127:305–316. https://doi.org/10.1016/j.cell.2006.08.046.
52. Ch'ng TH, Enquist LW. 2005. Neuron-to-cell spread of pseudorabies virus in a compartmented neuronal culture system. J Virol 79:10875–10889. https://doi.org/10.1128/JVI.79.17.10875-10889.2005.
53. Jansens RJJ, Van den Broeck W, De Pelsmaeker S, Lamote JAS, Van Waesberghe C, Couck L, Favoreel HW. 2017. Pseudorabies virus US3-induced tunneling nanotubes contain stabilized microtubules, interact with neighboring cells via cadherins, and allow intercellular molecular communication. J Virol 91:e00749-17. https://doi.org/10.1128/JVI.00749-17.
54. Favoreel HW, Van Minnebruggen G, Adriaensen D, Nauwynck HJ. 2005. Cytoskeletal rearrangements and cell extensions induced by the US3 kinase of an alphaherpesvirus are associated with enhanced spread. Proc Natl Acad Sci U S A 102:8990–8995. https://doi.org/10.1073/pnas.0409099102.
55. Brzozowska A, Rychłowski M, Lipińska AD, Bieńkowska-Szewczyk K. 2010. Point mutations in BHV-1 Us3 gene abolish its ability to induce cytoskeletal changes in various cell types. Vet Microbiol 143:8–13. https://doi.org/10.1016/j.vetmic.2010.02.008.
56. Delage E, Cervantes DC, Pénard E, Schmitt C, Syan S, Disanza A, Scita G, Zurzolo C. 2016. Differential identity of filopodia and tunneling nanotubes revealed by the opposite functions of actin regulatory complexes. Sci Rep 6:39632. https://doi.org/10.1038/srep39632.
57. Wild P, Engels M, Senn C, Tobler K, Ziegler U, Schraner EM, Loepfe E, Ackermann M, Mueller M, Walther P. 2005. Impairment of nuclear pores in bovine herpesvirus 1-infected MDBK cells. J Virol 79:1071–1083. https://doi.org/10.1128/JVI.79.2.1071-1083.2005.